ORIGINAL PAPER

Optimisation of parameters of complete nickel electrodeposition from acidic aqueous electrolytic baths prepared by dissolution of metal powder

M. Próchniak[1,2] · M. Grdeń[1,2]

Abstract

A methodology for electrochemical preparation of nickel layers intended to be used as targets for charged particle accelerators is proposed. The goal is to deposit the majority of metal dissolved in the electrolytic bath during a reasonable time (no longer than several hours) providing an acceptable quality of the deposits in terms of purity, surface roughness, compact and crack-free structure and mechanical stability. The electrodeposition is carried out from novel aqueous baths prepared by dissolution of a metal powder in a HNO_3-free solution due to the limited availability of isotopically enriched nickel concentration of the metal in the bath is low or moderate. This factor combined with the requirement of deposition of all dissolved metal makes serious differences between the target deposition and regular industrial plating. The impact of the electrolytic bath pH and the plating current density is analysed in order to optimise deposition parameters. The pH was varied from 3.8 to 5.3 while the applied current density ranged from 30 to 240 mA cm^{-2}. Progress in the deposition process was analysed using in situ UV–vis spectroscopy while a scanning electron microscope was applied to study the morphology of the deposits. Optimal electroplating conditions, which allow relatively fast deposition (up to ca. 7.2 h) of good quality metallic deposits containing most of the metal present in the bath ($\geq 95\%$), are suggested.

Keywords Nickel electrodeposition · Distribution diagrams · Electrolytic bath pH · Galvanostatic electrodeposition

Introduction

Electrochemically deposited nickel layers are frequently used as targets for the production of radioisotopes in accelerators [1–11]. Nuclear reactions of nickel nuclei with high energy charged projectiles, such as protons, deuterons or alpha particles, produce several copper and cobalt radioisotopes which found medical applications [12–15]. Generation of these radioisotopes usually relies on nuclear reactions of nickel isotopes of low natural abundance [15]. A high yield of such reactions is achieved when the target is highly enriched with a respective isotope.

There are several important factors that differ between electrochemical deposition of the accelerator targets and typical industrial plating used for the preparation of, e.g. protective layers. Firstly, nickel enriched isotopically is often very expensive, and usually, a limited amount of the metal is available for the preparation of the electrolytic bath. As a result, such prepared baths typically contain a moderate or small concentration of nickel cations (not higher than ca. 0.5 M) and/or the deposition is carried out from a small volume of the electrolyte, e.g. few millilitres [1, 6, 7, 15]. This is in contrast to typical industrial electroplating when the metal concentration in the bath is usually maintained at a level of moles per litre [16]. Furthermore, effective electrodeposition from such diluted baths requires the application of high current density. This entails the application of overpotentials located well within the hydrogen evolution region, a factor that is usually avoided in classical nickel electroplating.

Another important difference between industrial nickel electroplating and electrodeposition of the targets lies in the fact that the latter is carried out until the majority of the metal dissolved in the bath is deposited. This is in contrast to

✉ M. Próchniak
  mmieszkowska@chem.uw.edu.pl

✉ M. Grdeń
  mgrden@chem.uw.edu.pl

1 Faculty of Chemistry, University of Warsaw, Pasteura 1, 02-093 Warsaw, Poland

2 Biological and Chemical Research Centre, University of Warsaw, Żwirki i Wigury 101, 02-089 Warsaw, Poland

the classical industrial nickel electrodeposition which does not require deposition of all the metal dissolved in the bath. The amount of the nickel dissolved in the bath used for the target deposition is calculated in such a way that the deposition of all or almost all (e.g. > 95%) metal generates a target layer with the required thickness [1]. In contrast to typical approaches to the recovery of metals from electrolytes [17–19], the form of the deposited metal plays an important role here and the deposits in the form of powder or flakes are not accepted. Furthermore, high area 3D porous cathodes, such as foams [18–20], often used for effective metal recovery cannot be applied here and only flat and non-porous substrates are considered.

Deposition of the accelerator targets encounters additional difficulties related to the bath preparation. In contrast to the industrial electrolytes prepared by dissolution of nickel salts, the baths used for electrodeposition of the targets are very often prepared by dissolution of a metal powder. The latter is a common form of isotopically enriched nickel available on the market. Consequently, the selection of the method of the powder dissolution has a strong impact on the complexity of the bath preparation procedure. Thus, the solution resulting from the metal dissolution in concentrated HNO_3 contains the excess acid and the nitrates which may strongly affect the electrodeposition [21]. Therefore, these species are often removed from such prepared liquid by means of additional procedures, such as evaporation, precipitation and subsequent dissolution [2–5, 15, 22]. This, however, extends the bath preparation time and makes the procedure more complex.

In our previous paper [23], we reported a novel method of preparation of aqueous electrolytic baths which are intended for use for the deposition of the nickel targets for charged particle accelerators. The bath preparation method relies on the dissolution of the metal powder in a HNO_3-free solvent containing H_2SO_4 and H_2O_2. This is a simple and fast procedure and, in contrast to most of typically applied approaches [e.g. 3,4,5,9,10], does not require additional steps aimed at removal of the nitrates and the excess acid. The solution obtained from the metal dissolution is ready for further processing, i.e. dilution with water and the pH setting. The overall bath preparation procedure is therefore fast and simple and does not require sophisticated systems. Preliminary results show that these baths allow deposition of whole or almost whole (> 95%) amount of dissolved nickel within a reasonable time varying from ca. 3.5 to ca. 7 h, depending on the bath pH. This manuscript reports the results of extended studies aimed at optimisation of conditions of Ni deposition from the baths described in [23]. The novelty of the work includes analysis of the plating current density and the bath pH influence on complete Ni electrodeposition from the aforementioned newly developed electrolyte baths under conditions of limited electrolyte volume. Such analysis is

performed for the first time and, to the best of the authors' knowledge, there are no previously published works focusing on complete nickel electrodeposition from sulphate-acetate baths prepared by dissolution of metal nickel powder [19].

Experimental

The baths' preparation method was described in detail in [23]. Briefly, 50 ± 1 mg of metal Ni powder (Sigma Aldrich, 99.99%, particle size < 150 μm) was dissolved at room temperature (298 ± 1 K) in a chemical reaction in a mixture containing 0.5 ml of 3 M H_2SO_4 and 0.1 ml of 30% H_2O_2. The solution thus obtained was diluted with distilled water to a total volume of 2.0–2.1 ml. In our previous paper, we reported that neutralisation of such prepared solution with hydroxides or ammonia leads to the formation of a nickel precipitate, probably a double salt composed of $Ni(OH)_2$ and $NiSO_4$ which is reported to be hardly soluble in acids [24]. The other possibility includes the formation of a nickel kaliochalcite, an analogue to natrochalcite [25], although this compound is expected to exhibit higher solubility in mineral acids as compared to the $Ni(OH)_2$-$NiSO_4$ double salt [26]. The precipitate is dissolved using ammonia only at a sufficiently high pH (above 7). Therefore, the pH of the slightly acidic electrolyte was set up by adding a respective amount of $CH_3COONa \cdot 3H_2O$.

The final concentration of Ni^{2+} in the bath was equal to 0.41 ± 0.01 M. Deposition of the whole of the dissolved metal provides layers with the thickness of ca. 112–121 μm per 0.5 cm² of the geometric surface area of the electrode. The total concentration of sulphates and bisulphates in the bath was equal to 0.71 ± 0.03 M while the total content of all forms of acetates was varied from 0.82 to 3.69 M (pH from 3.8 to 5.3). In order to meet the requirements of high purity of the medical targets, the bath content should be limited to the necessary components only. Additives, such as surfactants or levellers, which may contaminate the deposit [27], should be avoided. H_3BO_3, which role in nickel electroplating is widely discussed in the literature [28–31] and which does not contaminate the deposit [1], is the only additive frequently added to the electrolytic baths in question. Its concentration was set up at 0.31 ± 0.01 M. The as-prepared bath contains also H_2O_2 which was not consumed during the metal powder reduction (concentration of ca. 70 mM) [23]. It is expected, however, that H_2O_2 is easily decomposed electrochemically during the plating process. The baths were prepared using water purified in a Millipore system (18.2 MΩ cm) and analytical grade purity chemicals (Avantor, B&K). The electrolysis was carried out under conditions of continuous gas evolution on both the cathode (H_2) and the anode (O_2) and no attempt was made to remove these gases from the

bath. The oxygen concentration is therefore expected to be higher than that in equilibrium with air [32] but is limited by the high ionic strength of the bath [33]. It was reported that the presence of oxygen in the electrolyte bath has no significant impact on nickel deposits plated at potentials of excessive hydrogen evolution [34].

The deposition was carried out at room temperature (298 ± 1 K) in a galvanostatic mode with a current density varying from 30 to 240 mA cm^{-2} (in respect to the geometric area of the cathode). A two-electrode system was applied. Polycrystalline gold (99.9%, Mint of Poland) was used as a substrate for the deposition while Pt wire (99.99%, Mint of Poland) acted as a counter electrode [15]. A polystyrene cuvette acted as an electrode cell. The geometry of the system was optimised for UV–vis measurements (details in Sect. S1 in Supplementary material), and under applied conditions, the analysis mirrors averaged bulk Ni^{2+} content in the cuvette. Although such determined concentration differs from that near the electrode surface, the UV–vis results properly mirror the rate of Ni^{2+} removal from the bath. Advanced facilities used for the production of medical radioisotopes utilise the electrode cell incorporated into a highly specialised shuttle which fits a specified irradiation facility [e.g. 9,35]. Therefore, the final geometry of the plating system must be optimised for a given accelerator. In order to simplify the system and to reduce disturbances in spectrophotometric measurements, the measurements were carried out in unstirred electrolyte, as it is frequently done in the medical targets electrodeposition. The plating efficiency and rate can be improved by moving the electrolyte through stirring or by application of a flow-through cell [18, 35]. Such an experimental setup must be optimised for a given geometry of the cell. It is worth to mention that the release of bubbles of gases evolved at the electrodes may affect the transport of the electroactive species by means of convection [36] but this effect is less efficient than mechanical stirring. The overall procedure is designed for application in a microscale only and involves electrolyte volume and nickel mass typical for deposition of targets for medical accelerators. It is economically unprofitable when scaled up to industrial systems demanding the processing of high amounts of nickel.

A Rohde&Schwarz HMP2020 programmable power supply and a CHI Instruments CHI660D electrochemical analyser were used for the deposition. UV–vis spectra were recorded using a Shimadzu UV-1800 spectrometer. All absorbance values are background corrected. ED-XRF analysis was carried out with a Shimadzu 800HS2 system using a 50-kV exciting X-ray beam. Scanning electron microscopy (SEM) images were acquired using a LEO 435 VP system. pH measurements were carried out using a Schott Lab870 pH-meter and a SI Analytics BlueLine electrode.

# Results and discussion

Influence of the initial bath pH

Speciation of Ni^{2+} present in the baths

It has been shown in our previous paper that the quality of the nickel layers deposited from the weakly acidic baths is considerably better as compared to the plating from the alkaline electrolytes [23]. Therefore, we focused our current studies on the baths with initial bulk pH values from 3.8 to 5.3. It is important to note that the nickel electrodeposition is accompanied by significant changes in the bulk pH of the bath. Thus, when the initial bath pH is in the range of 4.3–4.8 the final value of this parameter drops to a level as low as 1.8–2.3 (deposition of $\geq 95\%$ of the metal at 60 mA cm^{-2}). This is in agreement with the results reported by other authors [1, 2]. An opposite effect is observed for the initial bath pH as high as 5.3. Under such conditions, the final pH value is as high as 7.7–8.2.

It important to stress that the measured bath acidity represents a value averaged for the whole electrolyte volume and differs from the pH value near the electrode surface during the deposition process [28, 37–40]. These local pH changes are caused by hydrogen evolution reaction, HER, which takes place on the cathode simultaneously with the nickel deposition, and by oxygen evolution, OER, taking place on the anode [18, 37, 38, 40]. The former reaction leads to an increase in the pH near the cathode while the latter results in an opposite effect near the anode surface. Other processes, such as H$_2$O$_2$ and O$_2$ reduction, seem to be less important here (see, [23] and further sections of the text). The local pH changes are reduced in the presence of H$_3$BO$_3$ but they are not completely suppressed [37, 40].

A contribution from the nickel reduction to the cathodic reactions leads to a reduction in the electric charge consumed by the HER. The latter becomes smaller than the one related to the OER and the pH decrease due to the OER is not counterbalanced by the acidity decrease caused by the HER. As a result, a net decrease in the pH is observed for the baths with the initial bulk pH < 5.3. The net acidity decrease observed for the bath with the initial bulk pH of 5.3 will be discussed further in the text. We did not apply additional procedures aimed to restore the pH value during the deposition, [7].

Figure 1 shows UV–vis spectra recorded for the electrolyte baths with initial pH from 3.8 to 5.3. For comparison, the figure also includes spectra for an acetate-free bath (pH of 0.7) and for a bath with a low acetate content (113.6 mg of CH$_3$COONa·3H$_2$O and pH of 1.5). The two latter electrolytes were prepared in the same manner as the other baths studied in this work. An analysis of the spectra shows that Ni signals at 395 and 660–720 nm are not affected by the bath pH.
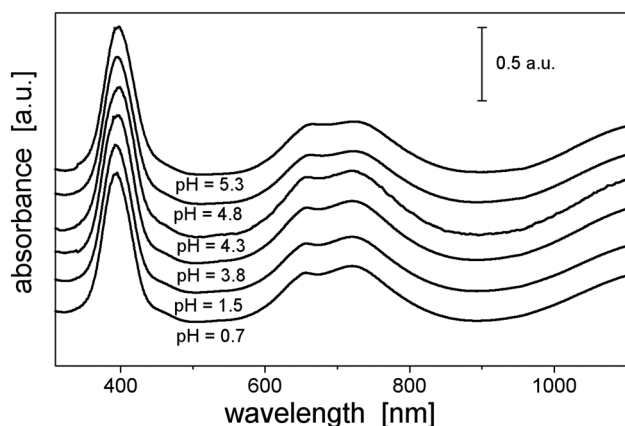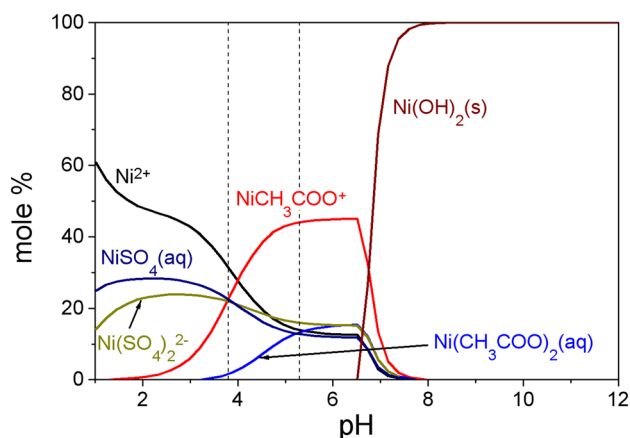
Fig. 1 UV–vis spectra recorded for the baths with various pH values indicated on the plot. The spectra are shifted along the horizontal axis for better readability

**Fig. 2** Distribution diagram for Ni^{2+} constructed for reactions and equilibrium constants listed in Table S1 (dataset no. 3) in Supplementary Materials. The electrolyte contains 0.41 M Ni^{2+}, 0.71 M H_2SO_4, 0.31 M H_3BO_3 and 1.38 M CH_3COONa. The sodium acetate concentration is the one averaged over the range analysed in this work. Ni^{2+} corresponds to hydrated nickel cations which do not form complexes with other than H_2O species bonded in a complex. Vertical broken lines correspond to the range of the initial pH values analysed in this work

The bath pH affects the chemistry of Ni^{2+} and, presumably also Ni^{+}, which is postulated as an unstable intermediate in the electrochemical reduction of divalent nickel cations [41–43]. It is important to stress that the electrolyte acidity is directly related to the acetate concentration in the electrolyte. These two factors act simultaneously and their influence on Ni^{2+} chemistry cannot be completely separated. Therefore, we report nickel speciation diagrams constructed for a given concentration of the acetates and for a wide range of the bath pH values. Such an approach allows tracking changes in Ni^{2+} chemistry when the electrolyte pH is altered during the electrodeposition.

Table S1 (supplementary material) collects the most important equilibria which involve chemical species present in the aqueous bath: Ni^{2+}, H_2SO_4, CH_3COONa and H_3BO_3. Due to the lack of data for complexes of the monovalent nickel cations, the analysis focuses on the divalent nickel only. The speciation diagrams were constructed using Medusa software [44, 45] on the basis of datasets collected in Table S1 and are shown in Figs. 2 and S3–S6 in Supplementary materials. The calculations were made for a typical electrolytic bath studied in this work containing Ni^{2+} (0.41 M), H_2SO_4 (0.71 M), H_3BO_3 (0.31 M) and CH_3COONa. The concentration of the latter varied from 0.82 to 3.69 M which corresponds to the pH range from 3.8 to 5.3 (averaged pH of 4.6 and concentration of 1.38 M). The molar strength of 1.9–3.7 was calculated on the basis of concentrations of ionic species formed by the dissolution of the respective chemical compounds.

An analysis of Figs. 2 and S3–S6 shows that the analysed baths contain soluble Ni^{2+} complexes: $[NiSO_4]$, $[Ni(SO_4)_2]^{2-}$, $[Ni(CH_3COO)]^{+}$ and $[Ni(CH_3COO)_2]$. The existence of these species was confirmed experimentally in [46–53]. Unfortunately, UV–vis data do not allow unambiguous distinction between complexes of Ni^{2+} with acetates and sulphates, as follows from a comparison of the spectra recorded in respective solutions [54–56]. When the bath pH is lower than ca. 6.5, the concentration of the acetate complexes of Ni^{2+} increases with a decrease in the electrolyte acidity. This is caused by pH-dependent dissociation of the acetic acid (Fig. S2) and is analogous to the effects observed for other weak organic acids [e.g. 57,58]. Because the initial bath pH is set up using the CH_3COONa, this effect corresponds to boosting the nickel complexation by the acetates when the concentration of the latter is raised [59]. This scenario changes when the initial pH is reduced to the value of 3.8. Under such conditions, the Ni^{2+} ions are complexed mainly by the sulphates and this effect is caused by both low pH value and low concentration of the acetates used for pH setting.

pH influence on plating time, faradaic efficiency and the deposit quality

The studies on the initial bath pH influence on the nickel electrodeposition were carried out for plating current density of 60 mA cm^{-2}. The progress in the deposition process was tracked using in situ UV–vis detection of Ni^{2+} ions remaining in the bath. In contrast to other approaches, such as visual analysis of the bath colour [7, 9, 60] or by application of dedicated chemical tests [2], this methodology allows for determining the deposition endpoint without termination of the process. The absorbance was measured at ca. 395 nm [54–56]. In the course of the plating process, the intensity of the Ni^{2+} signals decreases with the deposition time without changes in the peak positions.
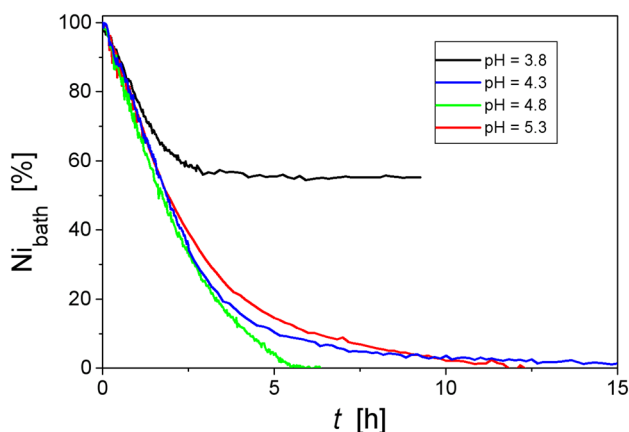
Fig. 3 Fraction of Ni remaining in the bath, Ni_{bath}, as a function of the deposition time for various initial bath pH values. The current density of 60 mA cm^{-2}, Ni_{bath} was calculated using Eq. (2) on the basis of in situ UV–vis measurements

The fraction of the nickel remaining in the bath, Ni_{bath}, at a time t counted from the start of the deposition was calculated using Eq. (1) [23]:

$$Ni_{bath}(t) = \frac{A(t)}{A_0} \cdot 100\% \tag{1}$$

where A_0 and $A(t)$ stand for the absorbance before (time = 0) and during the deposition (time = t), respectively. When the nickel dissolved in the bath is to be deposited completely, the amount of the deposit can be conveniently expressed as a percentage of the metal currently removed from the bath, Ni_{dep}, defined by Eq. (2):

$$Ni_{dep}(t) = 100 - Ni_{bath}(t) \tag{2}$$

The plots depicting changes in Ni_{bath} are shown in Fig. 3. They allow estimating the plating time required for the deposition of a certain mass of the metal. These values are collected in Table 1. An analysis of data presented in Fig. 3 and Table 1 clearly shows that the plating rate increases with the initial bath pH increase when the latter is lower than 5.3. The

least efficient is the bath with a pH of 3.8. It allows depositing of no more than ca. 45% of the metal during the plating time as long as 9 h. After this time, the bath pH drops to the value of 1.6. An increase in the rate of Ni^{2+} removal with the electrolyte pH increase was reported for acidic solutions containing Ni^{2+} concentrations as low as 15 mM [61].

The faradaic efficiency (current efficiency) of the deposition process, φ, is calculated for a given time window which spans from t_1 to t_2 (Δt) and is defined by Eq. (3) [62]:

$$\varphi = \frac{w}{M} \frac{nF}{Q_m} \cdot 100\% \tag{3}$$

where F is the Faraday constant, n stands for the number of the electrons exchanged in the Ni^{2+} reduction reaction ($n = 2$) and M is the molar mass of the metal. The total charge passed within the time window of Δt is equal to Q_m and this is accompanied by deposition of the metal with the mass equal to w. The in situ UV–vis measurements allow calculating the efficiency at any time of the plating process without its termination. Equation (3) is then transformed into Eq. (4):

$$\varphi(t_2) = \left[\left(\frac{A(t_1) - A(t_2)}{A_0} \right) N_0 \right] \frac{nF}{Q_m} \cdot 100\% \tag{4}$$

where N_0 denotes number of Ni moles initially present in the bath. A_0 is the absorbance measured before the experiment while $A(t_1)$ and $A(t_2)$ represent absorbances at the time of t_1 and t_2, respectively. The first term in the brackets in Eq. (4) represents number of moles of deposited metal and replaces the w/M ratio from Eq. (3). φ values calculated for Δt equal to 100 s are collected in Table 1 for selected Ni_{dep} values. The latter directly correspond to the plating time. Relatively low-efficiency values are attributed to a contribution from hydrogen evolution which takes place simultaneously with the Ni^{2+} reduction [18]. In general, the efficiency is weakly affected by the plating time up to Ni_{dep} of ca. 30%. It should be stressed that the UV–vis measurements provide information on the variation of the averaged bulk Ni^{2+} content and are less sensitive when the concentration changes are

Table 1 Faradaic deposition efficiencies, φ, for various initial bath pH values as a function of the progress in the plating process, Ni_{dep}. Plating current density of 60 mA cm^{-2}, φ was calculated using Eq. (4) for $\Delta t = 100$ s (details in the text). Reported values are averaged over several runs

Initial bath pH	Ni_{dep}							Estimated time required to deposit 95% of the metal dissolved in the bath (h)
	5%	10%	30%	40%	50%	75%	90%	
	φ at a time corresponding to a given Ni_{dep} value (%)							
3.8	38 ± 4	41 ± 2	31 ± 2	13 ± 3				n/a*
4.3	46 ± 3	47 ± 3	45 ± 3	43 ± 3	39 ± 3	24 ± 3	7 ± 3	7.2 ± 0.5
4.8	48 ± 3	49 ± 3	46 ± 3	42 ± 3	38 ± 3	24 ± 3	13 ± 4	4.9 ± 0.3
5.3	41 ± 4	42 ± 4	41 ± 4	38 ± 4	34 ± 4	17 ± 4	5 ± 4	8.5 ± 0.5

*Maximum amount of the metal deposited after ca. 9 h of plating is equal to ca. 44.8%

limited to a volume close to the cathode surface. The latter occurs at a short deposition time and may lead to an apparent lowering of the φ values calculated for the initial deposition stages, e.g. for Ni_{dep} of ca. 5%. When the deposition time is sufficiently long, the Ni^{2+} concentration in the bath becomes so low that a continuous decrease in φ is observed, in agreement with [17, 63]. The efficiency decrease is accelerated at Ni_{dep} higher than ca. 50%. Table 1 indicates that for the pH range from 4.3 to 4.8 the bath acidity has no significant impact on φ. A significant decrease in the efficiency is observed when the bath pH is as low as 3.8 and as high as 5.3, although in the latter case this effect is evident when the Ni_{dep} exceeds 50%. As compared to other baths with similar pH used for the Ni targets deposition, the efficiencies listed in Table 1 are similar to those described in [1] but lower than the ones reported in [2]. In general, these φ values are significantly lower than those typical for plating from industrial baths, both acidic and alkaline [16, 63, 64]. The decline in the faradaic efficiency with the bath acidity increase observed for pH lower than ca. 4 corresponds well to other reports [59, 63].

An analysis of Table 1 leads to important conclusions related to the changes in the bath pH in the course of the plating process. The results show that even at advanced stages of the plating process, such as the deposition of 40% of the metal, the Faradaic efficiency remains different for the baths with different initial pH. This indicates that the baths with various initial acidities differ in respect to the near-cathode pH for a relatively long time.

SEM images (Fig. 4) reveal a similar surface morphology for the initial bath pH of 4.3 and 4.8. These deposits are metallic in appearance, mechanically stable and of good quality. They strongly adhere to the substrate and do not peel off. Their surfaces are relatively smooth and free of cracks and possess only a small amount of spherical features. The formation of the latter may be explained by a deposition model which assumes that new layers are formed via the generation and subsequent coalescence of nuclei on a previously formed layer [65, 66]. It is expected that the spherical features in question are formed at the final stages of the diffusion-limited deposition when the concentration of the nickel in the bath goes down to a very low level and only a small number of nucleation centres is formed. An ED-XRF analysis (Fig. 5 and [23]) reveals that the layers deposited from the baths with an initial pH lower than 5.3 do not contain detectable amounts of other than nickel elements. The surface of these deposits is metallic as follows from an analysis of the voltammetry curve shown in Sect. S6 in Supplementary Material. A comparison with SEM images reported for electrodeposited Ni layers applied as the accelerator targets [1, 4, 22] suggests that the deposits with morphology depicted in Fig. 4b, c should meet the requirements of the accelerator production of medical isotopes. It follows

that prepared Ni layers can be used as deposited without further processing.

Setting the initial bath pH to a value outside the 4.3–4.8 range strongly affects the deposit quality. When the initial bath pH is as low as 3.8, the deposit covers the substrate surface non-uniformly (Fig. 4a). Deposition from the bath with a pH of 5.3 is faster than for lower pH values (Fig. 3) but it leads to the formation of poor quality deposits (Fig. 4d). Their surface is very rough and contains numerous cracks and loosely adherent fragments. This deposit is brittle and its small, powder size fragments are easily peeled off from the electrode. Some sections of the deposit are greenish indicating the presence of precipitated Ni(II) compounds. This is confirmed by an ED-XRF analysis (Fig. 5) which shows that, in contrast to the baths with lower pH values, the deposit plated at the pH of 5.3 contains significant amounts of sulphur, sodium and probably oxygen (sulphur escape peak and O Kα line overlap [67]). The compounds in question can be identified as $Ni(OH)_2$ with incorporated sulphates and Na^+ [68–70] or as a double salt-containing $Ni(OH)_2$ and $NiSO_4$ [24]. The top, greenish layers of this deposit are immediately removed by dissolution in concentrated HNO_3. This reveals the existence of a nickel deposit with a metallic appearance beneath the Ni^{2+} salt/hydroxide precipitate. It is worth to stress that the deposition from the baths with the initial pH of 5.3 is poorly reproducible and a green suspension is sometimes present also in the electrolyte.

Precipitation of the nickel salt/hydroxide from the bath with the initial pH of 5.3 has several important consequences. Firstly, the removal of a fraction of Ni^{2+} from the bath through a non-faradaic precipitation reduces the electric charge consumed by the metal reduction. This in turn increases HER contribution to the cathodic current and leads to a higher increase in pH near the electrode surface. As a result, the final acidity of the bath in question is significantly lower as compared to the baths with lower initial pH values. It may be suggested that the presence of the nickel hydroxide/salt precipitate may drive reactions which result in an additional electrolyte acidity decrease leading to the final increase in the bath pH. As for now, however, it is hard to identify such processes. The other important factor related to the formation of solid Ni-containing precipitates is removal of Ni^{2+} from the bath by means of precipitation not accompanied by charge transfer. This leads to an overestimation of φ calculated using Eq. (4). Under such conditions, the "true" faradaic efficiency at advanced stages of the process accompanied by the precipitate formation can be significantly lower than the values reported in Table 1.

The above-presented results show that the plating process is very sensitive to the initial bath pH. Formation of good quality deposits within a reasonable time period is possible only for the bath pH higher than 3.8 and lower than 5.3, e.g. from 4.3 to 4.8. When the initial bath pH is too high (e.g.
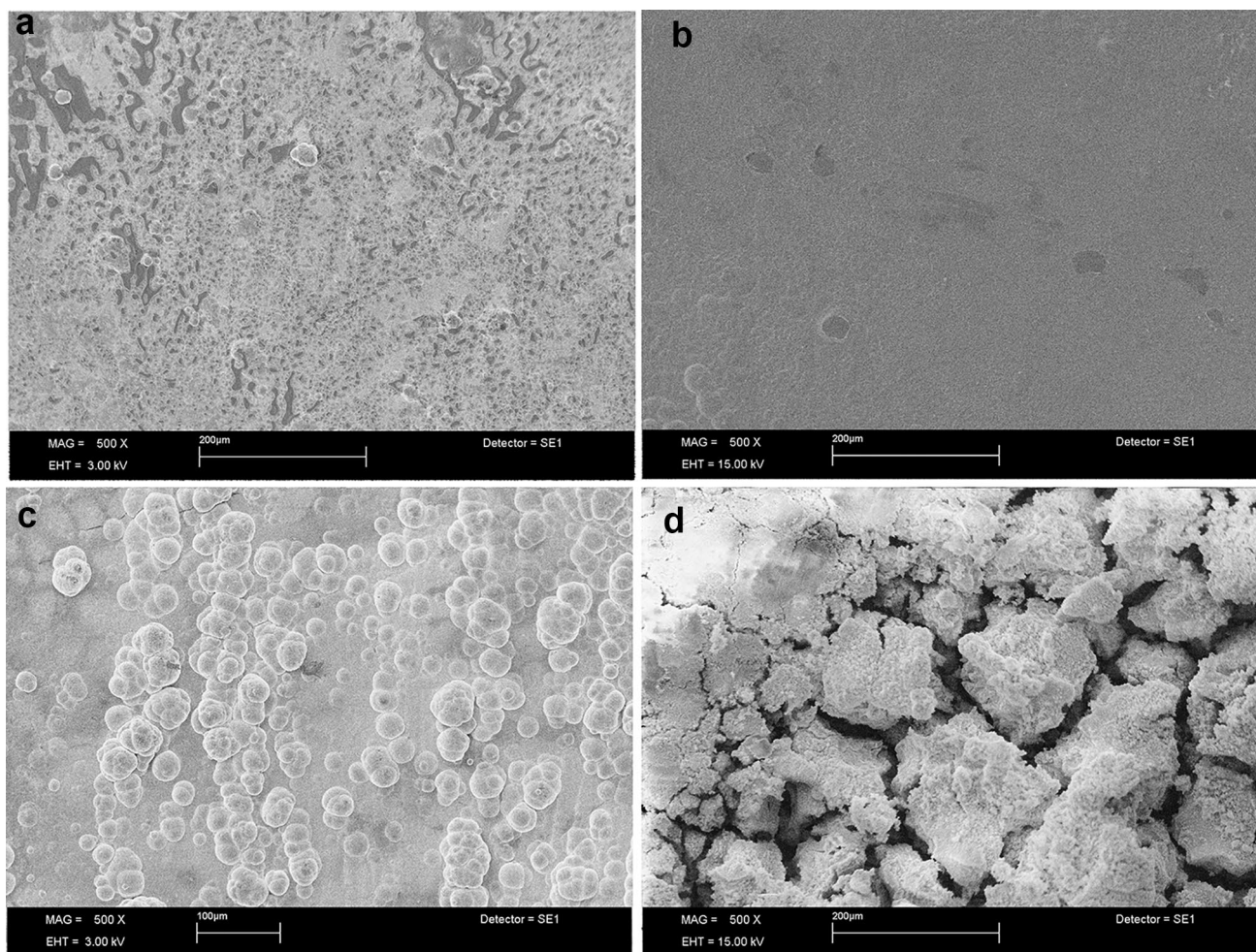
Fig. 4 Scanning electron microscopy images of Ni deposits plated from the baths with various initial pH values. Plating current density of 60 mA cm^{-2}, magnification of 500×. **a** pH = 3.8; **b** pH = 4.3; **c** pH = 4.8; **d** pH = 5.3. The images were taken for the deposits containing ≥ 95% (**b**, **c** and **d**) and ca. 45% (**a**) of the metal dissolved in the bath

5.3) quality of the deposit is very poor while for too low pH (e.g. 3.8), the plating process becomes very slow and the substrate coverage with the deposit is incomplete. This pH range differs from the one optimal for the Watts and the sulfamate baths [16]. The latter baths allow efficient nickel deposition at a pH lower than 3.8 while the upper pH limits are similar to the values find by us.

The bath pH influence on the nickel electroplating and its removal from the electrolyte was investigated in numerous works [e.g. 37,39,58,61,71–77]. The factors which are expected to be affected by the bath acidity include the overpotentials of faradaic reactions, the chemistry of the nickel ions present in the bath and the course of non-faradaic side processes, such as adsorption of various species at the electrode surface and formation of Ni(OH)$_2$ deposit. As a result, the bath pH influences the kinetics of the metal reduction [75] and properties of the deposit (texture, grain size or lattice constant) [39, 71, 75–78]. Some of these aspects are briefly discussed below.

An analysis of the bath pH influence on faradaic processes starts with the selection of cathodic reactions taking place in the system. Hydrogen evolution reaction, HER, is the most important reduction reaction simultaneous to nickel reduction [18]. The contribution of reduction of O$_2$ [18, 34, 79, 80] may be disregarded because this process is expected to be diffusion controlled at potentials of Ni deposition [81] and it is reported that its rate is significantly retarded when adsorbed hydrogen is present at the electrode surface [82]. Adsorbed hydrogen is generated at the nickel surface at potentials of HER although the surface coverage of nickel with this species is hard to quantify unambiguously [83]. Furthermore, oxygen solubility in solutions with high ionic strength, such as the analysed baths, is expected to be low [33]. Therefore, we focus our analysis only on the Ni^{2+} reduction and HER. The following discussion is based on Pourbaix and speciation diagrams which are of thermodynamic nature and do not provide exact kinetic and
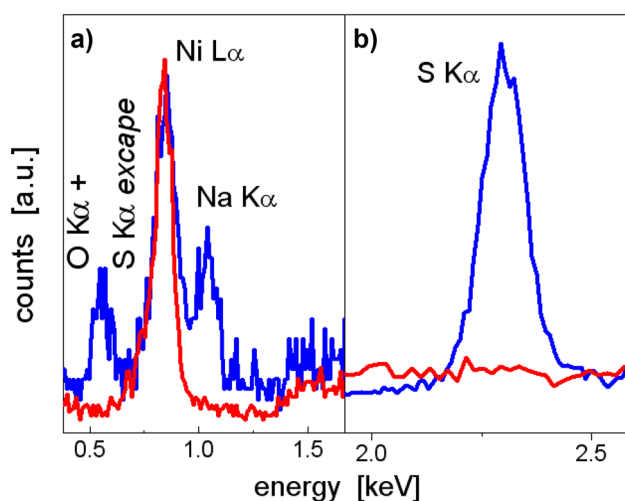
Fig. 5 ED-XRF spectrum recorded for a Ni deposit plated from a bath with a pH of 5.3 at 60 mA cm^{-2} (blue line). For comparison, a typical spectrum recorded for deposits obtained for lower pH values examined (≤ 4.8) is also shown (red line). **a** Oxygen region; **b** sulphur region

concentration data. They allow, however, analysing whether the rates of two parallel reactions, i.e. HER and Ni^{2+} reduction, evolve in the same manner when the bath pH and the current density are varied. They provide information on the bath pH-driven changes in the chemistry of Ni^{2+} which, in turn, are expected to affect the rate of the metal reduction. Therefore, the analysis presented below is of qualitative nature only but it helps to understand observed phenomena.

Figure 6 [77, 84, 85] shows a Pourbaix diagram constructed for Ni^{2+}/Ni and H^{+}(H$_2$O)/H$_2$ red-ox couples for standardised H$_2$ fugacity and Ni^{2+} activity, both equal to unity. It should be stressed, however, that the latter values
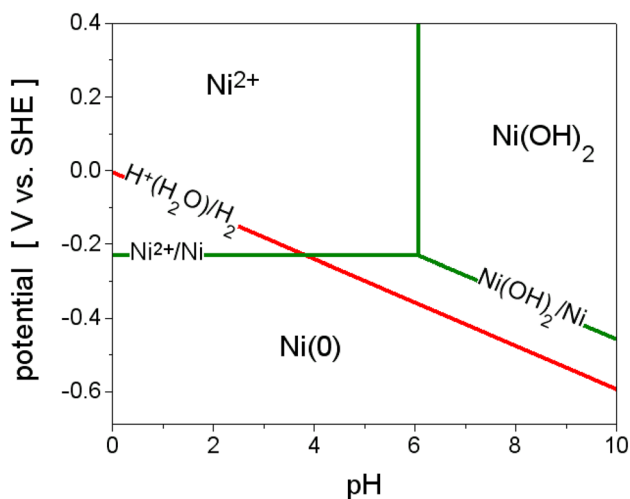
Fig. 6 Pourbaix diagram for H^{+}(H$_2$O)/H$_2$ and Ni^{2+}/Ni systems (after [77, 84, 85])

differ from the ones which are real for the analysed electrolytic baths. Therefore, in the system studied, the lines representing true equilibria in Ni^{2+}/Ni and H^{+}(H$_2$O)/H$_2$ red-ox couples should be shifted towards lower and higher potential values, respectively [86]. It follows that at pH lower than ca. 6 the bath acidity does not influence reversible potentials, E_r, of Ni/Ni^{2+} red-ox couple but affects the E_r of the H^{+}/H$_2$ (H$_2$O/H$_2$) system. This suggests that under galvanostatic conditions the contribution from the HER current, j_{HER}, to the total electric charge decreases with the pH increase. This is valid as long as both considered currents, i.e. j_{HER} and Ni^{2+} reduction current, i_{Ni}, are controlled exclusively or partially by the charge transfer kinetics. j_{HER}, is under kinetic control all the time [83, 87] while Ni^{2+} reduction is expected to evolve from the kinetic control to a mixed diffusion-kinetic regime [88, 89] and, finally, to pure diffusional control. At the initial stages of the deposition when the nickel reduction is completely or partially controlled by the charge transfer, the j_{Ni} to j_{HER} ratio increases with the bath pH [39]. Thus, it is likely that poor results of than deposition at pH of 3.8 can be partially attributed to vigorous HER at the beginning of the plating process. Additionally, gas bubbles generated during such vigorous reaction may block the substrate surface to a higher extent as compared to the lower bath pH values (Fig. 4a).

The chemistry of Ni^{2+} is practically unaffected by the electrolyte acidity when the latter contains only inorganic ligands, such as chlorides or sulphates, and when pH is higher than ca. 2 [90–93]. Experiments carried out with such type of solutions show a change in shape of voltammetric curves between pH values of 4 and 4.5 [73]. This effect was attributed to a competition between various species which inhibit the metal deposition, i.e. adsorbed hydrogen and/or Ni(OH)$_2$ [73, 77, 78, 94]. It was also shown [58, 63, 75, 77] that in the chloride and sulphate baths free from pH-dependent ligands the kinetics of the deposition process and the deposit properties evolve rather smoothly with the bath acidity. This is in contrast to the results shown in Figs. 3 and 4 and in Table 1 which point out to an abrupt change in course of the plating process for the pH values between 3.8 and 4.3. A similar effect was observed for, e.g. citrate baths, when the chemistry of Ni^{2+} changes significantly in a narrow pH range due to the formation of complexes with the organic ligand [58]. An analysis of Figs. 2 and S3–S6 shows that the baths which provide good quality deposits in a relatively short time (pH range from 4.3 to 4.8, Figs. 4 and 5) contain a significant fraction of Ni^{2+} (at least 40%) bonded in an acetate complex (Figs. 6, S3 and S4). The inhibition of the plating process observed for the bath pH of 3.8 corresponds to a lesser importance of Ni^{2+} complexation by the acetates due to lower bath pH and due to diminished overall concentration of CH$_3$COONa. This suggests that the

complexation of divalent nickel by the acetates has a beneficial role in the metal deposition. In fact, experimental evidence confirms that the presence of the acetates in the electrolyte may have a positive impact on nickel electrodeposition [95], although too high concentration of these anions (high pH values in the discussed baths) may lead to the formation of cracks in the deposits [96, 97]. The stability constants of Ni^{2+} complexes with the acetates are generally lower than for the sulphates (Table S1) and this would promote decomposition of $[Ni(CH_3COO)_n]^{(2-n)+}$ species facilitating the plating process [98]. Furthermore, the surface of the cathode subjected to a high cathodic polarisation is expected to be negatively charged. Electrostatic interactions of such a surface with anions, like $Ni(SO_4)_2^{2-}$, should impose additional hindrances to the discharging/adsorption of the latter. Unfortunately, we cannot discuss the influence of the complexing agents on Ni^+ intermediates [91, 99, 100] due to the lack of respective data.

The formation of the complexes is expected to affect also diffusion of Ni^{2+} ions [57, 101]. To the best of the author's knowledge, there are no published data which compare the diffusivity of Ni^{2+} complexes with the acetates and with the sulphates. This effect can be analysed in a simplified way using the Stokes–Einstein equation which assumes an inverse proportionality between the diffusion coefficient, D, and the radius of the diffusing species of a spherical shape [102]. The acetate radius is ca. 59% smaller than that of the sulphate (162 vs. 258 pm [103]). Consequently, the acetate complex of Ni^{2+} should exhibit D higher than the one with the sulphates when the same number of coordinating ligands is considered. This, in turn, indicates that the deposition process controlled exclusively or partially by diffusion should proceed faster when Ni^{2+} exists as an acetate complex.

Other than the above-discussed phenomena which are possibly pH dependent may include the formation and release of H_2 bubbles which screen the electrode surface [104–106]. This effect can be affected by the bath pH influence on the gas solubility in the electrolyte [107] or by the electrolyte composition impact on the surface wettability [76, 108]. The bath pH also affects number of nickel nuclei formed at the electrode surface [74] and may influence the adsorption of the acetic acid at the electrode surface. There is, however, not enough data as to further discuss importance of such effects.

The above discussion leads to a conclusion that a combination of two effects, i.e. the pH influence on the overpotentials of the cathodic reactions and on the chemistry of the nickel species present in the bath is responsible for the deterioration of the plating process at the initial bath pH as low as 3.8. At the early stages of the plating process, the bath pH influence on the reactions overpotentials plays an important role but at longer times, when the nickel reduction becomes diffusion controlled, the most important is probably the chemistry of Ni^{2+} species which, in turn, depends on the bath acidity and the acetates content.

The above-presented scenario which assumes that the increase in the bath pH is beneficial for the plating process cannot explain the formation of poor quality deposits when the initial bath pH is equal to 5.3. This effect can be understood if we consider the local pH increase near the cathode surface caused by the hydrogen evolution [38]. This may result in $Ni(OH)_2$ precipitation [18, 72, 109, 110] providing that the local pH increase is sufficiently high. Figure 2 indicates that a nickel hydroxide precipitate is formed at a pH above 6. It is likely that for the initial bulk pH as high as 5.3 the local acidity near the cathode may be reduced to a level sufficiently low as for triggering $Ni(OH)_2$ precipitation. When the initial bulk electrolyte pH is lower than 5.3 the increase in the local acidity does not reach the level required for the formation of $Ni(OH)_2$ precipitate and the entirely metallic deposits are formed.

When the deposit plated at a pH of 5.3 is dissolved in concentrated HNO_3 the existence of a metallic deposit below the Ni(II) compounds layer is revealed (pH influence on plating time, faradaic efficiency and the deposit quality). This indicates that the precipitation of the nickel salt/hydroxide takes place after a time delay long enough as to sufficiently increase the pH near the cathode surface [72, 109, 110]. An analysis of Table 1 confirms this conclusion. Thus, at early stages of the plating process (Ni_{dep} from 5 to 50%), the faradaic efficiency is very similar for the baths with the initial pH of 5.3 and of 4.3–4.8. This is changed when the extent of the deposited metal is as high as ca. 75%. Under such conditions, the efficiency decreases for the pH bath of 5.3 and this indicates serious hindrances in the electrodeposition process.

Influence of the current density

The influence of the current density, j, on the nickel deposition was analysed mainly for a single pH value of 4.3 which provides good quality deposits (Fig. 4). Figure 7 presents the rate of Ni^{2+} removal from the bath (Eq. (2)) for various j values while respective faradaic efficiencies (Eq. (2)) are collected in Table 2. As expected, the plating rate increases with the current density. Plating at j as low as 30 mA cm^{-2} results in a very slow deposition and no more than ca. 79% of the metal is deposited during 8.3 h. This current density also provides the lowest faradaic efficiencies. For higher j values and advanced stages of the process ($Ni_{dep} \geq 25\%$) the efficiency slightly increases with the current density.

An analysis of SEM images (Figs. 8 and 4b) shows that the quality of the deposits deteriorates when the current density is too high. The surfaces of the deposits obtained
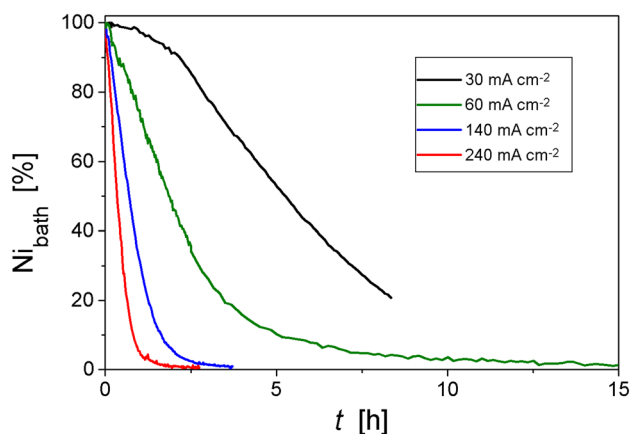
Fig. 7 Fraction of Ni remaining in the bath, Ni$_{bath}$, as a function of the current density. The initial bath pH of 4.3 (60–240 mA cm^{-2}) and 4.5 (30 mA cm^{-2}). Ni$_{bath}$ was calculated in the same manner as for Fig. 3

at j higher than 60 mA cm^{-2} contain more spherical features as compared to the lower deposition currents. Furthermore, the mechanical stability of the layers deposited at 240 mA cm^{-2} is poor and powder size fragments of the deposit are easily peeled off. It follows that the influence of the current density on the morphology of nickel layers deposited under conditions described in this work (Figs. 8 and 4b) is more pronounced as compared to the industrial Ni plating carried out using more concentrated baths and/or completed without significant depletion of the electrolyte [111–113]. Nevertheless, it can be concluded that the layers shown in Figs. 8a, b and 4b have a morphology similar to other Ni accelerator targets reported in the literature [1, 22].

The faradaic efficiency decreases with the plating time increase for all applied current densities when Ni$_{dep}$ is as high as 50%. Although the effect of the reduction of the deposition time due to the plating current increase is easy to explain intuitively, the current density influence on the faradaic efficiency (Table 2) requires a more thorough analysis.

Application of a higher cathodic current shifts the overpotentials of the respective reduction reactions towards more cathodic values. The values of separate currents of contributing reactions, i.e. j_{HER} and j_{Ni}, depend on their reversible potentials and on how the reaction rates are affected by the overpotential (Tafel slope, kinetic or diffusional control, etc.). When simultaneous reactions of the nickel reduction and the hydrogen evolution are considered, it is apparent that an increase in the plating current facilitates the establishment of pure diffusional control of the metal reduction process. This factor is expected to increase the ratio of j_{HER} to j_{Ni}. However, the extensive hydrogen evolution at a higher current density should increase pH near the electrode surface to a higher extent as compared to the lower applied j values [38]. This is partially confirmed by the fact that the final pH measured after completing the electrodeposition slightly increases with the plating current: from ca. 2.1 for 60 mA cm^{-2} to 2.7 for 140 mA cm^{-2} and, finally, to 3.9 for 240 mA cm^{-2} (the same initial bath pH of 4.3). As it was discussed earlier, such an increase in pH can be beneficial for the nickel deposition process and it may somewhat impede hydrogen evolution due to changes in the overpotential of this reaction (Fig. 6). As a result, the faradaic efficiency increases with j providing that the latter has a sufficiently high value. It is likely that at too high current densities the pH near the cathode surface may rise to a level sufficiently high as to precipitate Ni(OH)$_2$ [40]. On the other hand, an increase in the current density leads to a more extensive gas evolution taking place on both electrodes. This factor may lead to a more efficient bath stirring by gas bubbles which, in turn, may reduce pH increase near the cathode. Low φ values calculated for the lowest j applied (30 mA cm^{-2}) can be explained by the fact that the cathode polarisation at such a low current is significantly smaller than for the higher j values. Under such conditions, the nickel deposition process is expected to be very slow and is strongly suppressed by HER. After a sufficiently long deposition time, the local pH near the cathode becomes sufficiently high to facilitate the metal deposition. This effect is mirrored in Fig. 7 by an

Table 2 Faradaic deposition efficiencies, φ, for various plating current densities as a function of the progress in the plating process, Ni$_{dep}$. φ was calculated using Eq. (4) for $\Delta t = 100$ s (details in the text), initial bath pH of 4.3 except 30 mA cm^{-2} (pH of 4.5). Reported values are averaged over several runs

Current density (mA cm^{-2})	Ni$_{dep}$						Estimated time required to deposit 95% of the metal dissolved in the bath (h)
	5%	10%	25%	50%	75%	90%	
	φ at a time corresponding to a given Ni$_{dep}$ value (%)						
30[a]	17±2	36±2	46±3	39±3	25±4		n/a[b]
60	46±3	47±3	49±3	39±3	24±3	7±3	7.2±0.5
140	45±2	47±3	51±2	46±2	29±2	13±2	2.0±0.3
240	50±2	47±2	57±2	54±2	34±2	15±2	1.0±0.2

[a]pH of 4.5

[b]Maximum amount of the metal deposited after ca. 8.3 h of plating is equal to ca. 79%
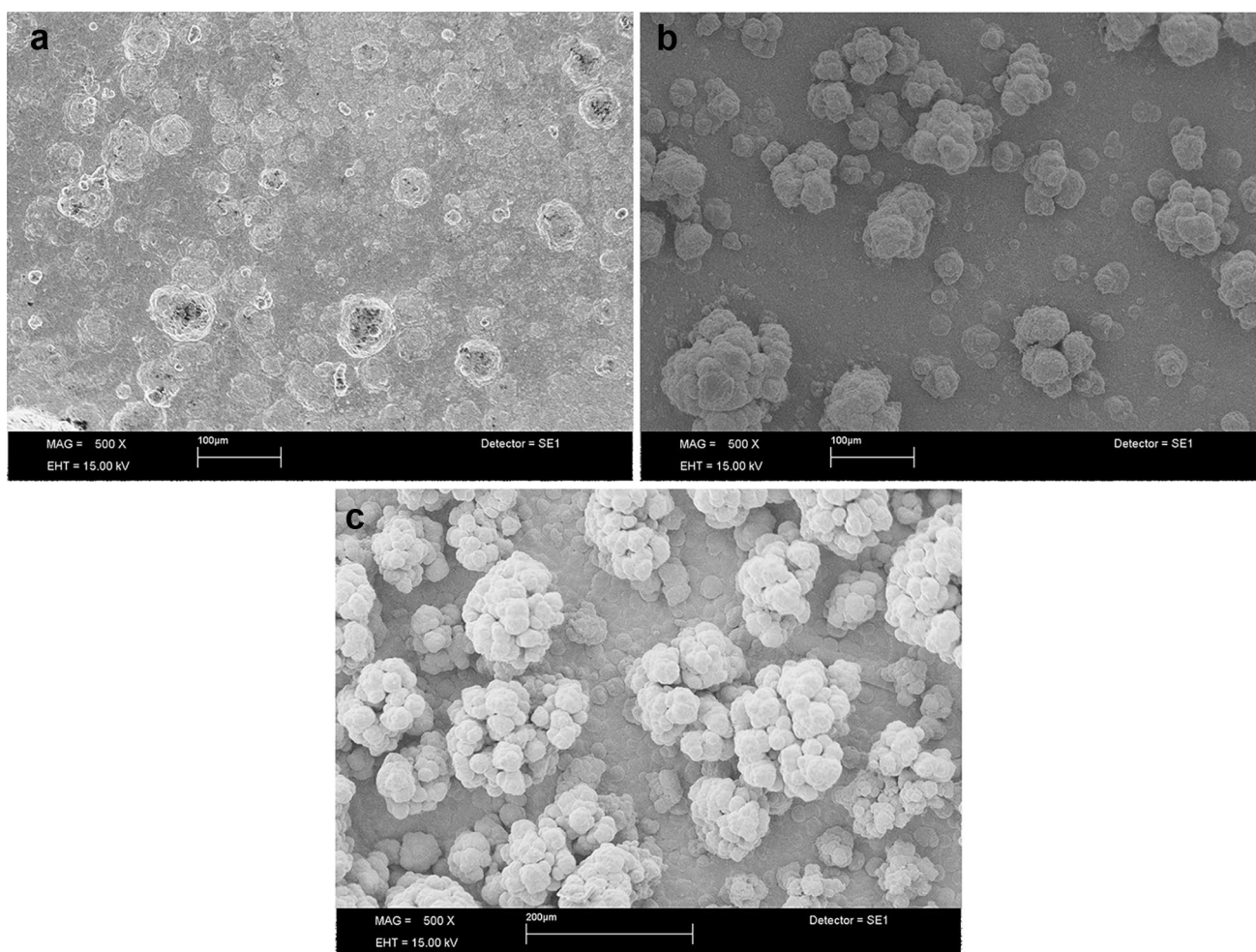
Fig. 8 Scanning electron microscopy images of Ni deposits plated at various current densities. Magnification of $500\times$. **a** 30 mA cm^{-2}; **b** 140 mA cm^{-2}; **c** 240 mA cm^{-2}. The SEM image for 60 mA cm^{-2} is shown in Fig. 4b. Initial bath pH of 4.3 (**b** and **c**) and 4.5 (**a**). The images were taken for the deposits containing $\geq 95\%$ (**b**, **c**) and ca. 79% (**a**) of the metal dissolved in the bath

increase in the Ni^{2+} removal rate after an induction time when the deposition rate is very small.

In summary, the above-presented analysis allows determining optimal conditions of complete Ni electrodeposition carried out from the analysed baths. Good quality deposits which may found application as accelerator targets are plated from the baths with pH ranging from 4.3 to 4.8 and for the deposition currents from 60 to 140 mA cm^{-2}. Application of these parameters allows deposition of ca. 95% of the metal within 2–7.2 h, depending on the bath pH and the current density.

Conclusions

Nickel layers with a thickness of up to ca. 100 µm are obtained by complete electrochemical deposition from novel baths prepared by dissolution of metallic Ni powder in a HNO$_3$-free solvent. The layers are intended to be used as targets for accelerator production of isotopes and their deposition requires complete or almost complete removal of metal dissolved in the bath. The work focuses on the optimalisation of deposition conditions which allow the preparation of good quality deposits containing at least 95% of nickel deposited in the bath during a reasonable plating time. Various initial pH values of the bath, ranging from 3.8 to 5.3, are obtained by the addition of respective amounts of CH$_3$COONa. The plating was accomplished by application of a constant current density in the range of 30–240 mA cm^{-2}. The progress in the deposition process was tracked using in situ UV–vis spectrometry. The deposition rate and the faradaic efficiency increase both with the bath pH and with the current density. The quality of the deposit, on the other hand, deteriorates when the bath pH and the current density are too high. Too low initial bath pH results in serious retardation of the plating process and non-uniform substrate coverage with the

deposit. The most important factors which are expected to affect pH influence on the deposition process are the bath acidity-dependent shifts in the reversible potentials of the respective reactions and complexation of nickel ions present in the electrolyte.

References

1. Rajec P, Csiba V, Leporis M, Štefečka M, Losonczi Pataky E, Reich M, Ometáková J (2010) Preparation and characterization of nickel targets for cyclotron production of ^{64}Cu. J Radioanal Nucl Chem 286:665–670

2. Manrique-Arias JC, Avila-Rodriguez MA (2014) A simple and efficient method of nickel electrodeposition for the cyclotron production of ^{64}Cu. Appl Radiat Isotop 89:37–41

3. McCarthy DW, Shefer RE, Klinkowstein RE, Bass LA, Margeneau WH, Cutler CS, Anderson CJ, Welch MJ (1997) Efficient production of high specific activity ^{64}Cu using a biomedical cyclotron. Nucl Med Biol 24:35–43

4. Kim JY, Park H, Lee JC, Kim KM, Lee KC, Ha HJ, Choi TH, An GI, Cheon GJ (2009) A simple Cu-64 production and its application of Cu-64 ATSM. Appl Radiat Isotop 67:1190–1194

5. Ohya T, Nagatsu K, Suzuki H, Fukada M, Minegishi K, Hanyu M, Fukumura T, Zhang MR (2016) Efficient preparation of high-quality ^{64}Cu for routine use. Nucl Med Biol 43:685–691

6. Avila-Rodriguez MA, Nye JA, Nickles RJ (2007) Simultaneous production of high specific activity ^{64}Cu and ^{61}Co with 11.4MeV protons on enriched ^{64}Ni nuclei. Appl Radiat Isotop 65:1115–1120

7. Zeisler SK, Pavan RA, Orzechowski J, Langlois R, Rodrigue S, van Lier JE (2003) Production of ^{64}Cu on the Sherbrooke TR-PET cyclotron. J Radioanal Nucl Chem 257:175–177

8. Adam Rebeles R, Van den Winkel P, Hermanne A, Tárkányi F (2009) New measurement and evaluation of the excitation function of ^{64}Ni(p, n) reaction for the production of ^{64}Cu. Nucl Instr Met Phys Res B 267:457–461

9. Burke P, Golovko O, Clark JC, Aigbirhio FI (2010) An automated method for regular productions of copper-64 for PET radiopharmaceuticals. Inorg Chim Acta 363:1316–1319

10. Jauregui-Osoro M, De Robertis S, Halsted P, Gould SM, Yu Z, Paul RL, Marsden PK, Gee AD, Fenwick A, Blower PJ (2021) Production of copper-64 using a hospital cyclotron: targetry, purification and quality analysis. Nucl Med Commun 42:1024–1038

11. Pfeifer A, Knigge U, Mortensen J, Oturai P, Kiil Berthelsen A, Loft A, Binderup T, Rasmussen P, Elema D, Levin Klausen T, Holm S, von Benzon E, Højgaard L, Kjaer A (2012) Clinical PET of Neuroendocrine Tumors Using ^{64}Cu-DOTATATE: First-in-Humans Study. J Nucl Med 53:1207–1215

12. Smith SV, Jones M, Holmes V (2011) Production and selection of metal PET radioisotopes for molecular imaging. In Singh N (ed) Radioisotopes - applications in bio-medical science. InTech, Rijeka, pp 199–224

13. Spellerberg S, Reimer P, Blessing G, Coenen HH, Qaim SM (1998) Production of ^{55}Co and ^{57}Co via proton induced reactions on highly enriched ^{58}Ni. Appl Radiat Isot 49:1519–1522

14. Boros E, Packard AB (2019) Radioactive Transition Metals for Imaging and Therapy. Chem Rev 119:870–901

15. Mieszkowska M, Grdeń M (2021) Electrochemical deposition of nickel targets from aqueous electrolytes for medical radioisotope production in accelerators: a review. J Solid State Electrochem 25:1699–1725

16. Di Bari GA (2001) Electrodeposition of nickel. In: Schlesinger M, Paunovic M (eds) Modern electroplating. Wiley, Hoboken, pp 79–114

17. Avci E (1989) Electrolytic recovery of nickel from dilute solutions. Separat Sci Techn 24:317–324

18. Walsh FC, Reade GW (1994) Electrochemical techniques for the treatment of dilute metal-ion solutions. In Sequeira CAC (ed) Studied in environmental science. Environmental Oriented Electrochemistry. Elsevier, New York, pp 3–44

19. Coman V, Robotin B, Ilea P (2013) Nickel recovery/removal from industrial wastes: a review. Resour Conserv Recy 73:229–238

20. Maarof HI, Daud WMAW, Aroua MK (2017) Recent trends in removal and recovery of heavy metals from wastewater by electrochemical technologies. Rev Chem Eng 33:359–386

21. Streinz CC, Hartman AP, Motupally S, Weidner JW (1995) The effect of current and nickel nitrate concentration on the deposition of nickel hydroxide films. J Electrochem Soc 142:1084–1089

22. Xie Q, Zhu H, Wang F, Meng X, Ren Q, Xia C, Yang Z (2017) Establishing reliable Cu-64 production process: from target plating to molecular specific tumor micro-PET imaging. Molecules 22:641–1–641–10

23. Próchniak M, Grdeń M (2022) Electrochemical deposition of nickel from aqueous electrolytic baths prepared by dissolution of metallic powder. J Solid State Electrochem 26:431–447

24. Saarinen T, Lindfors LE, Fugleberg S (1996) A study of a nickel hydroxide sulphate precipitate obtained during hydrogen reduction of nickel hydroxide slurries. Hydrometallurgy 43:129–142

25. Krickl R, Wildner M (2007) Crystal chemistry of synthetic Co- and Ni-analogues of natrochalcite – the shortest known hydrogen bonds among mineral-type compounds. Part I: Single-crystal X-ray structures. Eur J Mineral 19:805–816

26. Anthony JW, Bideaux RA, Bladh KW, Nichols MC (2005) Handbook of mineralogy. Mineralogical Society of America, Chantilly

27. Schlesinger M, Paunovic M (2001) Modern electroplating. Wiley, Hoboken

28. Tsuru Y, Nomura M, Foulkes FR (2002) Effects of boric acid on hydrogen evolution and internal stress in films deposited from a nickel sulfamate bath. J Appl Electrochem 32:629–634

29. Šupicová M, Rozik R, Trnková L, Oriňáková R, Gálová M (2006) Influence of boric acid on the electrochemical deposition of Ni. J Solid State Electrochem 10:61–68

30. Zech N, Landolt D (2000) The influence of boric acid and sulfate ions on the hydrogen formation in Ni-Fe plating electrolytes. Electrochim Acta 45:3461–3471

31. Song KD, Kim KB, Han SH, Lee HK (2003) A study on effect of hydrogen reduction reaction on the initial stage of Ni electrodeposition using EQCM. Electrochem Commun 5:460–466

32. Wang JG, Shi L, Su Y, Liu L, Yang Z, Huang R, Xie J, Tian Y, Li D (2021) In-situ plasmonic tracking oxygen evolution reveals multistage oxygen diffusion and accumulating inhibition. Nature Commun. https://doi.org/10.1038/s41467-021-22434-3

33. Xing W, Yin M, Lv Q, Hu Y, Liu C, Zhang J (2014) Oxygen solubility, diffusion coefficient, and solution viscosity. In: Xing

W, Yin G, Zhang J (eds) Rotating electrode methods and oxygen reduction electrocatalysts. Elsevier, Amsterdam, pp 1–31

34. Gui CQ, Lee JY (1995) Nickel deposition from unbuffered neutral chloride solutions in the presence of oxygen. Electrochim Acta 40:1653–1662

35. Matarrese M, Bedeschi P, Scardaoni R, Sudati F, Savi A, Pepe A, Masiello V, Todde S, Gianolli L, Messa C, Fazio F (2010) Automated production of copper radioisotopes and preparation of high specific activity [^{64}Cu]Cu-ATSM for PET studies. Appl Radiat Isot 68:5–13

36. Chen Y, Mojica F, Li G, Abel Chuang PY (2017) Experimental study and analytical modeling of an alkaline water electrolysis cell. Int J Energy Res 1–9

37. Ji J, Cooper WC, Dreisinger DB, Peters E (1995) Surface pH measurements during nickel electrodeposition. J Appl Electrochem 25:642–650

38. Obata K, van de Krol R, Schwarze M, Schomäcker R, Abdi FF (2020) In situ observation of pH change during water splitting in neutral pH conditions: impact of natural convection driven by buoyancy effects. Energy Environ Sci 13:5104–5116

39. Ritzert NL, Moffat TP (2016) Ultramicroelectrode studies of self-terminated nickel electrodeposition and nickel hydroxide formation upon water reduction. J Phys Chem C 120:27478–27489

40. Balakai VI, Arzumanova AV, Balakai KV (2010) Alkalization of the near-cathode layer in electrodeposition of nickel from a chloride electrode. Russ J Appl Chem 83:65–71

41. Oriňáková R, Strečková M, Trnková L, Rozik R, Gálova M (2006) Comparison of chloride and sulphate electrolytes in nickel electrodeposition on a paraffin impregnated graphite electrode. J Electroanal Chem 594:152–159

42. Santana AIC, Díaz SL, Barcia OE, Mattos OR (2009) A kinetic study on nickel electrodeposition from sulfate acid solution. II Reaction modeling J Electrochem Soc 156:D331–D335

43. Oriňáková R, Turoňová A, Kladeková D, Gálová M, Smith RM (2006) Recent developments in the electrodeposition of nickel and some nickel-based alloys. J Appl Electrochem 36:957–972

44. Chemical Equilibrium Diagrams, KTH Royal Institute of Technology, Department of Chemistry, available at https://www.kth.se/che/medusa (Accessed on 01 May 2022)

45. Páez-Hernández ME, Ramírez MT, Rojas-Hernández A (2000) Predominance zone diagrams and their application to solvent extraction techniques. Talanta 51:107–121

46. Gamsjäger H, Bugajski J, Gajda T, Lemire RJ, Preis W (2005) Chemical thermodynamics of nickel. Chemical thermodynamics, Vol. 6. Elsevier, Amsterdam

47. Strathmann TJ, Myneni SCB (2004) Speciation of aqueous Ni(II)-carboxylate and Ni(II)-fulvic acid solutions: Combined ATR-FTIR and XAFS analysis. Geochim Cosm Acta 68:3441–3458

48. Schröder D, Ducháčková L, Tarábek J, Karwowska M, Fijalkowski KJ, Ončák M, Slavíček P (2011) Direct observation of triple ions in aqueous solutions of nickel(II) sulfate: a molecular link between the Gas phase and bulk behavior. J Am Chem Soc 133:2444–2451

49. Chen T, Hefter G, Buchner R (2005) Ion association and hydration in aqueous solutions of nickel(II) and cobalt(II) sulfate. J Solut Chem 34:1045–1066

50. Duplâtre G, Haessler A, Marques Netto A (1984) Ion association studies in aqueous NiSO$_4$ solutions by positron lifetime spectroscopy. J Radioanal Nucl Chem 82:219–228

51. Bickley RI, Edwards HGM, Rose SJ, Gustar R (1990) A Raman spectroscopic study of nickel(II) acetate, Ni(CH$_3$COO)$_2$ and its aqueous and methanolic solutions. J Mol Struct 238:15–26

52. Bonsen A, Eggers F, Knoche W (1976) Formation of nickel acetate complexes. Inorg Chem 15:1212–1215

53. Fuentes R Jr, Morgan LO, Matwiyoff NA (1975) Fourier transform carbon-13 nuclear magnetic resonance of aqueous nickel(II)-acetic acid solutions. I. equilibrium quotients from relative abundances of solution species. Inorg Chem 14:1837–1840

54. Mech K (2017) Influence of organic ligands on electrodeposition and surface properties of nickel films. Surf Coat Technol 315:232–239

55. Wang J, Gabe DR, Hart AC, Crouch PC (2013) The chemistry of nickel electroplating solutions. Trans IMF 91:4–10

56. Petrova EV, Vorontsova MA, Manomenova VL, Rashkovich LN (2012) Some properties of aqueous solutions of α-NiSO$_4$·6H$_2$O. Crystallogr Rep 57:579–584

57. Rudnik E, Wojnicki M, Włoch G (2012) Effect of gluconate addition on the electrodeposition of nickel from acidic baths. Surf Coat Technol 207:375–388

58. Tadashi T, Mizumoto K, Tanaka S, Yamashita T (2004) Effect of bath pH on nickel citrate electroplating bath. Met Finish 102:104–111

59. Srinivasan R, Ramesh Bapu GNK (2011) Characterisation of nickel deposits from nickel acetate bath. Trans IMF 89:275–280

60. Ometáková J, Rajec P, Csiba V, Leporis M, Štefečka M, Vlk P, Galamboš M, Rosskopfova O (2012) Automated production of ^{64}Cu prepared by 18 MeV cyclotron. J Radioanal Nucl Chem 293:217–222

61. Grimshaw P, Calo JM, Shirvanian PA, Hradil G (2011) II. Electrodeposition/removal of nickel in a spouted electrochemical reactor. Ind Eng Chem Res 50:9525–9531

62. Pletcher D, Walsh FC (1993) Industrial electrochemistry. Springer, Heidelberg

63. Robotin B, Ispas A, Coman V, Bund A, Ilea P (2013) Nickel recovery from electronic waste II Electrodeposition of Ni and Ni–Fe alloys from diluted sulfate solutions. Waste Manag 33:2381–2389

64. Fornari P, Abbruzzese C (1999) Copper and nickel selective recovery by electrowinning from electronic and galvanic industrial solutions. Hydrometallurgy 52:209–222

65. Guo L, Searson PC (2010) On the influence of the nucleation overpotential on island growth in electrodeposition. Electrochim Acta 55:4086–4091

66. Gamburg YD, Zangari G (2011) Theory and practice of metal electrodeposition. Springer, London

67. Verma HR (2007) Atomic and nuclear analytical methods. Springer, Heidelberg

68. Hall DS, Lockwood DJ, Bock C, MacDougall BR (2015) Nickel hydroxides and related materials: a review of their structures, synthesis and properties. Proc R Soc A 47:20140792–1–20140792–65

69. McBreen J (1990) The nickel oxide electrode. In: Bockris J'OM, White RE, Conway BE (eds) Modern Aspects of Electrochemistry, Vol 21. Plenum Press, New York, pp 29–64

70. Cordoba-Torresi SI, Gabrielli C, Hugot-Le Goff A, Torresi R (1991) Electrochromic behavior of nickel oxide electrodes: I. Identification of the colored state using quartz crystal microbalance. J Electrochem Soc 138:1548–1553

71. Motoyama M, Fukunaka Y, Sakka T, Ogata YH (2006) Effect of surface pH on electrodeposited Ni films. J Electrochem Soc 153:C502–C508

72. Lantelme F, Seghiouer A, Derja A (1998) Model of nickel electrodeposition from acidic medium. J Appl Electrochem 28:907–913

73. Proud WG, Gomez E, Sarret E, Valles E, Müller C (1995) Influence of pH on nickel electrodeposition at low nickel(II) concentrations. J Appl Electrochem 25:770–775

74. Xu Y, Zhu Z, Liu L, Liu Z (2021) Electrochemical study of nickel nucleation mechanisms on glassy carbon at different pH values in an industrial electrolyte. Int J Mater Res 112:143–149

75. Piatti RCV, Arvía AJ, Podestá JJ (1969) The electrochemical kinetic behaviour of nickel in acid aqueous solutions containing chloride and perchlorate ions. Electrochim Acta 14:541–560

76. Yue B, Zhu G, Wang Y, Song J, Chang Z, Guo N, Xu M (2022) Research on wettability of nickel coating changes induced in the electrodeposition process. J Electroanal Chem 910:116–146

77. Boubatra M, Azizi A, Schmerber G, Dinia A (2012) The influence of pH electrolyte on the electrochemical deposition and properties of nickel thin films. Ionics 18:425–432

78. Amblard J, Epelboin I, Froment M, Maurin G (1979) Inhibition and nickel electrocrystallization. J Appl Electrochem 9:233–242

79. Ferreira EB, Tahmasebi S, Jerkiewicz G (2021) On the catalytic activity and corrosion behavior of polycrystalline nickel in alkaline media in the presence of neutral and reactive gases. Electrocatalysis 12:146–164

80. Bagotzky VS, Shumilova NA, Samoilov GP, Khrushcheva EI (1972) Electrochemical oxygen reduction on nickel electrodes in alkaline solutions-II. Electrochim Acta 17:1625–1635

81. Wang J, Zhao CX, Liu JN, Ren D, Li BQ, Huang JQ, Zhang Q (2021) Quantitative kinetic analysis on oxygen reduction reaction: a perspective. Nano Mater Sci 3:313–318

82. Gómez-Marín AM, Rizo R, Feliu JM (2013) Some reflections on the understanding of the oxygen reduction reaction at Pt(111). Beilstein J Nanotechnol 4:956–967

83. Lasia A, Rami A (1990) Kinetics of hydrogen evolution on nickel electrodes. J Electroanal Chem 294:123–141

84. Pourbaix M (1974) Atlas of electrochemical equilibria in aqueous solutions. NACE, Houston

85. Beverskog B, Puigdomenech I (1997) Revised Pourbaix diagrams for nickel at 25–300°C. Corr Sci 39:969–980

86. Jerkiewicz G (2020) Standard and reversible hydrogen electrodes: theory, design, operation, and applications. ACS Catal 10:8409–8417

87. Seri O (2017) Differentiating approach to the Tafel slope of hydrogen evolution reaction on nickel electrode. Electrochem Commun 81:150–153

88. Milchev A, Zapryanova T (2006) Nucleation and growth of copper under combined charge transfer and diffusion limitations. Part I Electrochim Acta 51:2926–2933

89. Mamme MH, Deconinck J, Ustarroz J (2017) Transition between kinetic and diffusion control during the initial stages of electrochemical growth using numerical modelling. Electrochim Acta 258:662–668

90. Hankin A, Kelsall GH (2012) Electrochemical recovery of nickel from nickel sulfamate plating effluents. J Appl Electrochem 42:629–643

91. Grujicic D, Pesic B (2006) Electrochemical and AFM study of nickel nucleation mechanisms on vitreous carbon from ammonium sulfate solutions. Electrochim Acta 51:2678–2690

92. Ji J, Cooper WC (1996) Nickel speciation in aqueous chloride solutions. Electochim Acta 41:1549–1560

93. Martí-Calatayud MC, García-Gabaldón M, Pérez-Herranz V, Ortega E (2011) Determination of transport properties of Ni(II) through a Nafion cation-exchange membrane in chromic acid solutions. J Membr Sci 379:449–458

94. Bergenstof Nielsen C, Horsewell A, Østergård MJL (1997) On texture formation of nickel electrodeposits. J Appl Electrochem 27:839–845

95. Marikkannu KR, Surya Kala K, Paruthimal Kalaignan G, Vasudevan T (2008) Electroplating of nickel from acetate based bath - Hull Cell studies. Trans IMF 86:172–176

96. Antikhovich IV, Chernik AA, Zharskii IM, Bolvako AK (2015) Electrodeposition of a nickel coating from a low-temperature acetate-chloride nickel-plating electrolyte. Rus J Electrochem 51:281–285

97. Dennis JK, Such TE (1993) Nickel and chromium plating. Woodhead, Cambridge

98. Standardized high current solid targets for cyclotron production of diagnostic and therapeutic radionuclides (2004) Technical Reports Series No. 432, IAEA, Vienna

99. Badea GE, Badea T (2008) Electrochemical behaviour of nickel in aqueous acetic acid solutions. Rev Roum Chim 53:291–295

100. Saraby-Reintjes A, Fleischmann M (1984) Kinetics of electrodeposition of nickel from Watts baths. Electrochim Acta 29:557–566

101. Buffle J, Zhang Z, Startchev K (2007) Metal flux and dynamic speciation at (bio)interfaces. Part I: Critical evaluation and compilation of physicochemical parameters for complexes with simple ligands and fulvic/humic substances. Environ Sci Technol 41:7609–7620

102. Koryta J, Dvořák J, Kavan L (1993) Principles of electrochemistry. Wiley, Chichester

103. Jenkins HDB, Thakur HP (1979) Reappraisal of thermochemical radii for complex ions. J Chem Educ 56:576–577

104. Fujimura T, Hikima W, Fukunaka Y, Homma T (2019) Analysis of the effect of surface wettability on hydrogen evolution reaction in water electrolysis using micro-patterned electrodes. Electrochem Commun 101:43–46

105. Pereiro I, Fomitcheva Khartchenko A, Petrini L, Kaigala GV (2019) Nip the bubble in the bud: a guide to avoid gas nucleation in microfluidics. Lab Chip 19:2296–2314

106. Meegoda JN, Hewage SA, Batagoda JH (2018) Stability of nanobubbles. Environm. Eng Sci 35:1216–1227

107. Ruetschi P, Amlie RF (1966) Solubility of hydrogen in potassium hydroxide and sulfuric acid. Salting-out and hydration J Phys Chem 70:718–723

108. Siddaiah A, Kumar P, Henderson A, Misra M, Menezes PL (2019) Surface energy and tribology of electrodeposited Ni and Ni–graphene coatings on steel. Lubricants 7:87–1–87–15

109. Khalil RM (1988) Electrodeposition of catalytically active nickel powders from electrolytes of various anionic compositions. J Appl Electrochem 18:292–297

110. Zhang JJ, Zhang TA, Feng S (2020) α-Ni(OH)$_2$ electrodeposition from NiCl$_2$ solution. Trans Nonferrous Met Soc China 30:2802–2811

111. Uhm YR, Park KY, Choi SJ (2015) The effects of current density and saccharin addition on the grain size of electroplated nickel. Res Chem Intermed 41:4141–4149

112. Rashidi AM (2012) A galvanostatic modeling for preparation of electrodeposited nanocrystalline coatings by control of current density. J Mater Sci Technol 28:1071–1076

113. Wasekar NP, Haridoss P, Seshadri SK, Sundararajan G (2016) Influence of mode of electrodeposition, current density and saccharin on the microstructure and hardness of electrodeposited nanocrystalline nickel coatings. Surf Coat Technol 291:130–140